Restricted Backbone Conformational and Motional Flexibilities of Loops Containing Peptidyl−Proline Bonds Dominate the Enzyme Activity of Staphylococcal Nuclease[†,‡]

Lu Shan, Yufeng Tong, Tao Xie, Min Wang, and Jinfeng Wang*

National Laboratory of Biomacromolecules, Center for Molecular Biology, Institute of Biophysics, Chinese Academy of Sciences, 15 Datun Road, Beijing 100101, China

Received May 22, 2007; Revised Manuscript Received August 10, 2007

ABSTRACT: The role of *cis*−*trans* isomerizations of peptidyl−proline bonds in the enzyme activity of staphylococcal nuclease (SNase) was examined by mutation of proline residues. The proline-free SNase ([Pro$^-$]SNase), namely, P11A/P31A/P42A/P47T/P56A/P117G-mutant SNase, was adopted for elucidating the correlation between the nuclease activity and the backbone conformational and dynamic states of SNase. The 3D solution structure of [Pro$^-$]SNase has been determined by heteronuclear NMR experiments. Comparing the structure of [Pro$^-$]SNase with the structure of SNase revealed the conformational differences between the two proteins. In the structure of [Pro$^-$]SNase, conformational rearrangements were observed for the loop of residues Ala112−His121 containing a *trans* Lys116−Gly117 peptide bond and for the C-terminal α-helical loop of residues Leu137−Glu142. Mutation of proline at position 117 also caused the conformational rearrangement of the p-loop (Asp77−Leu89), which is remote from the Ala112−His121 loop. The Ala112−His121 loop and p-loop are placed closer to each other in [Pro$^-$]SNase than in SNase. The backbone dynamic features of the *ω*-loop (Pro42−Pro56) of SNase are different from those of [Pro$^-$]SNase. The backbone of the *ω*-loop exhibits restricted flexibility with slow conformational exchange motions in SNase, but is highly flexible in [Pro$^-$]SNase. The analysis indicates that the restrained backbone conformation of the Ala112−His121 loop and restricted flexibility of the *ω*-loop are two dominant factors determining the enzyme activity of SNase. Of the two factors, the former is correlated with the strained *cis* Lys116−Pro117 peptide bond and the latter is correlated with the *cis*−*trans* isomerizations of the His46−Pro47 peptide bond.

Proline *cis*−*trans* isomerism makes significant contributions to protein folding and function. The intrinsically slow conformational steps, caused by *cis*−*trans* isomerizations of peptidyl−proline bonds (*1*) can give rise to conformational heterogeneity in protein folding, resulting in multiple parallel folding pathways. For some proteins, the proline *cis*−*trans* isomerism can play an important role in their biological functions (*2*). The significance of proline *cis*−*trans* isomerism in the folding and function of staphylococcal nuclease (SNase) has received considerable attention for several decades.

SNase is a protein having no cysteine residues or lacking disulfide bonds, but contains six proline residues at sequence positions 11, 31, 42, 47, 56, and 117. In the tertiary structure of SNase (*3*, *4*), Pro11 is in *β*-strand His8−Ala12, and Pro31 and Pro42 are residues adjacent to the C-terminal ends of *β*-turn *τ*2 (Tyr27−Gln30) and short *β*-strand V39−T41, respectively, whereas Pro56 adjoins the N-terminus of helix α1 (Ala58−Ala69). Pro47 and Pro117 are located in two loops, the *ω*-loop (Pro42−Pro56) and the loop of residues Ala112−His121, respectively. Measurable populations of *cis* and *trans* configurations have been detected at the Lys116−Pro117 and His46−Pro47 peptide bonds in SNase (*5*, *6*). Approximately 90% and 20% of the SNase molecules have a *cis* Lys116−Pro117 peptide bond and a *cis* His46−Pro47 peptide bond, respectively. The segment of residues Tyr115−Asn118 adopts a type I′ *β*-turn conformation with the Lys116−Gly117 peptide bond in the *trans*-isomer and a type VI_a *β*-turn conformation with the Lys116−Pro117 peptide bond in the *cis*-isomer. Extensive studies have contributed to the determination of the thermodynamic features of proline *cis*−*trans* isomerization and the structural properties that influence *cis*−*trans* equilibrium at the peptide bond Lys116−Pro117 (*7*−*12*). It was indicated that some conformational restrictions must be imposed on the segment containing the Lys116−Pro117 peptide bond. The stress which causes the strained *cis* Lys116−Pro117 peptide bond originates in the anchorage of the ends of the loop segment of residues Ala112−Pro117 by residues Val111 and Asn118 (*8*, *9*). The *cis*−*trans* isomerization of the Lys116−Pro117 peptide bond is the source of heterogeneous partially folded conformations of the 1−121 and 1−135 residue SNase fragments (*13*), suggesting multiple parallel folding pathways in the folding

[†] This research was supported by the National Natural Science Foundation of China (Grant NNSFC 30570375).

[‡] The atomic coordinates of [Pro$^-$]SNase have been deposited in the Protein Data Bank (accession code 2PQE), and the chemical shifts of [Pro$^-$]SNase have been deposited in BioMagResBank along with the associated NMR parameters (accession number 15232).

* To whom correspondence should be addressed. E-mail: jfw@sun5.ibp.ac.cn. Phone.: +86-10-64888490. Fax: +86-10-64872026.

10.1021/bi7009794 CCC: $37.00
Published on Web 09/22/2007

of SNase with chain elongation from residue K110 to the C-terminal region of the molecule in vitro. In the folding of the 1−79 residue SNase fragment (SNase79), the *trans*-isomer of the Gln30−Pro31 peptide bond is responsible for the nativelike folding of the segment Thr13−Val39, whereas the *cis*-isomer of the Gln30−Pro31 peptide bond causes SNase79 to be in an unfolded state (*14*). However, studies of the kinetics of folding and unfolding of the proline-free variants (*15*−*17*) have indicated that multiple parallel pathway folding was detected despite the absence of prolines in SNase. The fast folding phase corresponds to the refolding of the native proline isomer, and the middle folding phase may correspond to the slow refolding of the non-native proline isomer.

Although the effects of isomerizations of peptidyl−proline bonds on the stability and folding of SNase have been studied extensively, the influences of *cis*−*trans* isomerizations of peptidyl−proline bonds on the backbone conformation and dynamics of SNase as well as on nuclease activity have not been deciphered clearly. SNase from the Foggi strain of *Staphylococcus aureus* (SNase WT) and SNase from the V8 strain (SNase(V8)) show only one amino acid difference at position 124, that SNase WT contains His124 and SNase-(V8) contains Leu124. In the present study, we have adopted a proline-free SNase(V8), in which all six proline residues have been replaced by alanine or glycine/threonine. The solution structure and backbone dynamics of proline-free SNase(V8) were determined by heteronuclear NMR methods. The structural and dynamic features of proline-free SNase-(V8) were compared with those determined for SNase(V8). The effects of the *cis* and *trans* forms of the Lys116−Pro117 and His46−Pro47 peptide bonds on the conformational and dynamic features of the corresponding segments were described. The cause of the dramatic decrease in the enzyme activity of proline-free SNase(V8) was analyzed.

MATERIALS AND METHODS

Sample Preparation. The plasmid for expression of the proline-free SNase(V8) was constructed by creating one mutation at sequence position 124 along the gene of proline-free SNase WT. The proline-free SNase WT is a P11A/P31A/P42A/P47T/P56A/P117G-mutant wild-type SNase. The site-directed mutagenesis was performed using PCR-mediated megaprimer mutagenesis (*18*). SNase(V8) and proline-free SNase(V8) (we will call them SNase and [Pro$^-$]SNase, respectively, hereafter) were expressed and purified according to the procedures described previously (*19*). Uniformly ^{15}N-labeled SNase, uniformly ^{15}N- and ^{13}C- labeled [Pro$^-$]SNase, and ^{15}N/^{13}C-doubly-labeled [Pro$^-$]SNase were obtained through bacterial growth in M9 minimal medium using ^{15}-NH_4Cl (1 g/L) and ^{13}C-glucose (2 g/L) as the sole nitrogen and carbon sources. The purity of the proteins was checked by SDS−PAGE to be a single band. Samples of SNase and [Pro$^-$]SNase in 90% H_2O/10% D_2O containing 1 mM proteins, 100 mM KCl, and 50 mM deuterated acetate buffer (pH 5.0) were prepared for NMR experiments.

Nuclease Activity Assay. The enzyme activities of SNase and [Pro$^-$]SNase for hydrolysis of single-stranded DNA were measured with a Shimadzu UV-250 spectrophotometer by monitoring the increase in absorbance at 260 nm (*20*). The single-strand salmon sperm DNA, obtained by boiling salmon sperm DNA at 100 °C for 30 min and rapidly cooling it on ice, was used as a substrate of the measurements. The measurements were performed at 25 °C with enzymes in 1.0 mL of a solution containing 50 μg/mL denatured salmon sperm DNA, 25 mM Tris−HCl (pH 7.4), and 10 mM $CaCl_2$. One unit of enzymatic activity was defined as the amount of enzyme causing a change of 1.0 absorbance unit/min at 260 nm in a 1.0 cm cell.

NMR Spectroscopy. All NMR experiments were run on a Bruker DMX 600 spectrometer equipped with a triple-resonance cryoprobe at 300 K for SNase and [Pro$^-$]SNase. The 3D ^{1}H−^{15}N−^{13}C HNCO/HN(CA)CO, HNCA/HN(CO)-CA, and HNCACB/CBCA(CO)NH experiments for backbone resonance assignments were performed with a sample of [Pro$^-$]SNase. The 3D ^{1}H−^{15}N−^{13}C (H)CC(CO)NH/H(CCCO)NH, ^{1}H−^{13}C HCCH-TOCSY, ^{1}H−^{15}N TOCSY-HSQC, and ^{1}H−^{15}N−^{13}C HBHA(CO)NH experiments were carried out for the assignments of side chain resonances of [Pro$^-$]SNase. The 3D ^{1}H−^{15}N NOESY-HSQC and TOCSY-HSQC and ^{1}H−^{13}C NOESY-HSQC spectra of [Pro$^-$]SNase were collected with mixing times of 120, 60, and 120 ms, respectively (*21*, *22*). All the NMR data were processed and analyzed using FELIX98 (Accelrys Inc.). The data points in each indirect dimension were usually doubled by linear prediction (*23*) before zero filling to the appropriate size. A 90° to 60° shifted square sine bell apodization was used for all three dimensions prior to Fourier transformation. ^{1}H chemical shifts were referenced to internal 2,2-dimethyl-2-silapentane-5-sulfonate (DSS). ^{15}N and ^{13}C chemical shifts were referenced indirectly (*24*).

For the backbone dynamics studies, the 2D ^{15}N T_1 and T_2 HSQC and ^{1}H−^{15}N NOE experiments were performed with 1 mM SNase and [Pro$^-$]SNase at 300 K using standard methods (*25*). For ^{15}N T_1 measurements, the delay times were set to 12, 62, 142, 282, 382, 522, 822, 1202, and 1602 ms. For T_2 measurements, relaxation delays of 8.5, 17.0, 25.4, 33.9, 50.9, 67.8, 84.8, 101.8, 118.7, 135.7, and 152.6 ms were used. In the 2D ^{1}H−^{15}N NOE experiments a delay of 2 s was followed by ^{1}H saturation for 3 s, whereas the saturation period was replaced by a delay of equivalent duration in the control experiment. Two experiments were run in an interleaved manner.

Structure Calculation. The NOE cross-peaks between main chain protons, between side chain protons, and between main chain and side chain protons were identified for [Pro$^-$]SNase. The obtained medium- and long-range NOEs were used for determination of 3D structures of the protein. In the structure calculation, dihedral angle constraints were obtained using the program TALOS (*26*). Restraints of ±25° to ±60° were applied for ϕ and ψ angles. Hydrogen bond restraints were estimated by the slow H/D exchange data and the predicted secondary structures using the CSI protocol. The structures were calculated using the program CNS 1.1 (*27*) on Silicon Graphics station Onyx 2. A family of 200 structures was generated, from which a final set of the 20 best structures was considered for use in the analysis of structural statistics.

Determination of ^{15}N Relaxation Parameters. The ^{15}N relaxation rate constants R_1 and R_2 for each residue of SNase and [Pro$^-$]SNase were determined by nonlinear least-squares fitting of the intensities of the cross-peaks in the corresponding 2D NMR spectra to a monoexponential equation. The uncertainties in the peak heights were estimated from the

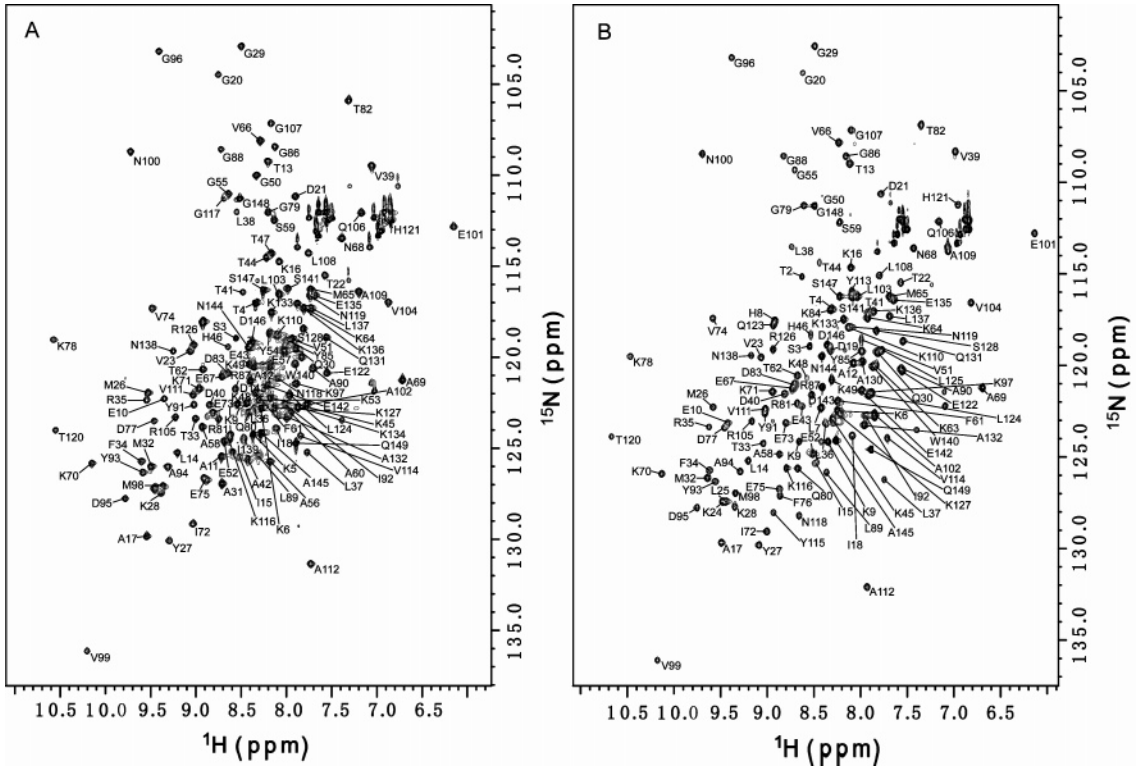

FIGURE 1: 2D ^{1}H−^{15}N HSQC spectra of [Pro^{-}]SNase (A) and SNase (B) in aqueous solution. NMR resonance assignments are given by the one-letter amino acid code and residue number.

root-mean-square value of the background noise regions (*28*). The ^{1}H−^{15}N NOE value was calculated as the ratio of peak intensities measured from the spectra acquired with and without irradiation during the recycle delay. The reported standard deviations for NOE values were obtained indirectly from the root-mean-square baseline noise or directly from two independent experiments. Analysis of the rotational diffusion tensor was performed using the program TENSOR 2.0 (*29*). The anisotropic diffusion parameters were calculated using a subset of residues that did not show significant increases in R_2 values and had NOE values >0.65. The overall tumbling correlation times estimated from R_2/R_1 ratios and axially symmetric diffusion tensor components $D_{\parallel}/D_{\perp}$ were 9.50 ns and 1.35 for SNase and 9.50 ns and 1.28 for [Pro^{-}]SNase, respectively. These diffusion parameters and the R_1, R_2, and ^{1}H−^{15}N NOE relaxation data were then used as the input for the model-free analysis (*30*). The model-free parameters were obtained following the same procedure as previously reported (*31*).

RESULTS

Enzymatic Activities. The nuclease activities of [Pro^{-}]SNase and SNase were measured at 25 °C to examine the effect of the P11A/P31A/P42A/P47T/P56A/P117G mutation on enzymatic function. The results reveal that the mutation of six prolines leads to a great decrease in the nuclease activity of [Pro^{-}]SNase. [Pro^{-}]SNase has only 1.4% of the activity of SNase. This means [Pro^{-}]SNase is almost inactive.

Changes in the Backbone Conformation of [Pro^{-}]SNase. The 2D ^{1}H−^{15}N HSQC spectra of [Pro^{-}]SNase (Figure 1A) and SNase (Figure 1B) show the assigned cross-peaks of amide groups of the proteins. For [Pro^{-}]Snase, 97%, 97%, 97%, and 99% of the backbone $^{1}H_N$, ^{15}N, $^{1}H_\alpha$, and $^{13}C_\alpha$ resonances were assigned, respectively. Cross-peaks of Tyr113 and Tyr115 cannot be observed in the 2D ^{1}H−^{15}N HSQC spectrum of [Pro^{-}]SNase. This may correlate to the great changes in backbone conformation around residues Tyr113 and Tyr115 due to the mutation of proline to glycine at position 117 of [Pro^{-}]SNase, since residues Tyr113 and Tyr115 are very close to the X−Pro peptide bond Lys116−Pro117 in the sequence position.

The chemical shifts of assigned resonances for [Pro^{-}]SNase were compared to those for SNase. Figure 2 shows the chemical shift differences of the $^{1}H_N$, ^{15}N, $^{1}H_\alpha$, and $^{13}C_\alpha$ resonances between [Pro^{-}]SNase and SNase ($\Delta^{1}H_N$, Δ^{15}N, $\Delta^{1}H_\alpha$, and $\Delta^{13}C_\alpha$). The locations of the residues showing remarkable chemical shift changes in the tertiary structure of SNase are shown in Figure 3. Apparently, the substitutions of alanines for prolines at sequence positions 11, 31, 42, and 56 and substitutions of threonine and glycine at residues Pro47 and Pro117, respectively, can cause chemical shift changes of nearby residues in the corresponding structural regions. Therefore, the explicit changes in the chemical shift of Glu10 having $\Delta(^{13}C_\alpha) > 1.5$ ppm and $\Delta(^{1}H_\alpha) > 0.2$ ppm is due to the mutation at residue Pro11 in the β-strand of residues His8−Ala12. Pro31 adjoining the C-terminal of β-turn τ2 (Tyr27−Gln30) is close in space to residues Leu25 and Tyr27. Thus, mutation at residue Pro31 caused large changes in the chemical shifts of residues Leu25 showing $\Delta(^{13}C_\alpha) > 4.0$ ppm, Tyr27 showing $\Delta(^{1}H_N) > 0.15$ ppm, Gln30 showing $\Delta(^{13}C_\alpha) > 1.5$ ppm and $\Delta(^{1}H_\alpha) > 0.3$ ppm, and Met32 showing $\Delta(^{1}H_N) > 0.2$ ppm. Pro56 adjoins the N-terminal of helix α1 (Glu57−Ala69) and is close to Ser59 in the helical conformation. Thus, substitution at Pro56 can cause changes in the chemical shifts of residue Ser59 as well as residues Tyr54 and Gly55. Ser59 shows $\Delta(^{15}N) > 1.0$

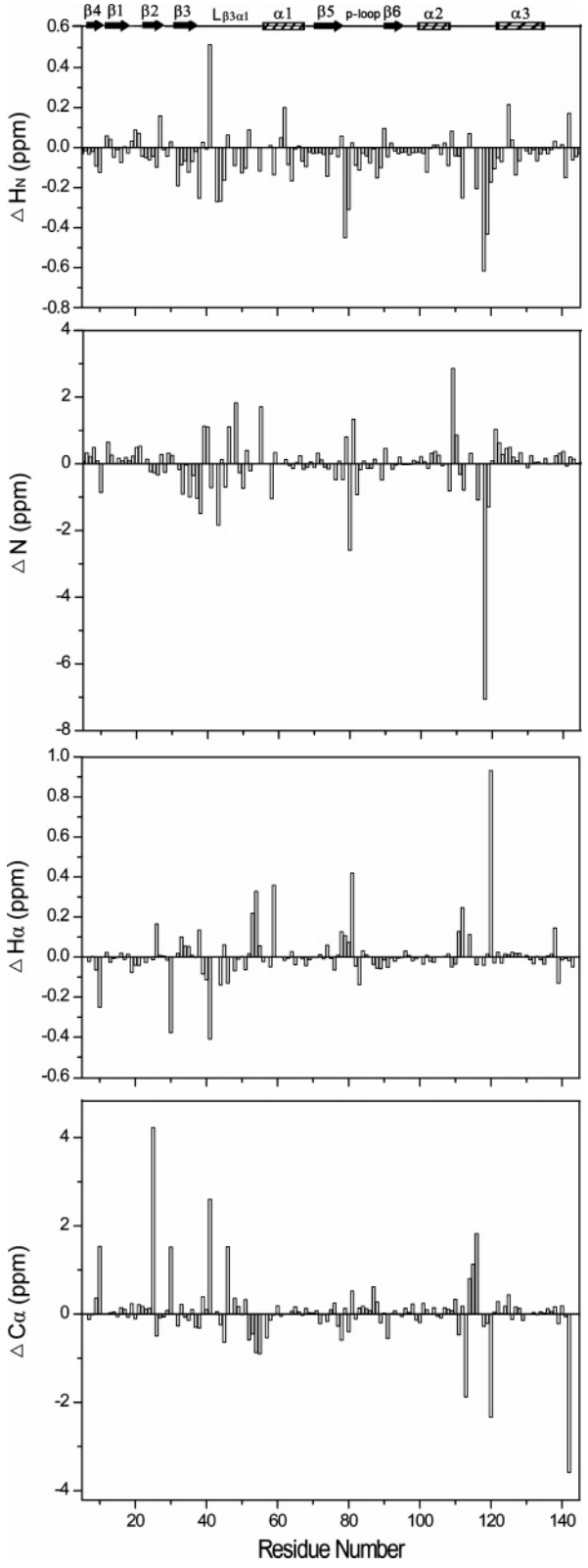

FIGURE 2: Histogram of chemical shift differences of ^{15}N, $^{1}H_N$, $^{13}C_\alpha$, and $^{1}H_\alpha$ resonances between [Pro$^-$]SNase and SNase. The secondary structural elements are indicated in the top of the diagram.

ppm and $\Delta(^1H_\alpha) > 0.3$ ppm, and Tyr54 and Gly55 show $\Delta(^1H_\alpha) > 0.3$ ppm and $\Delta(^{15}N) > 1.5$ ppm, respectively. The large chemical shift changes of Thr41 showing $\Delta(^1H_N) > 0.5$ ppm, $\Delta(^1H_\alpha) > 0.4$ ppm, and $\Delta(^{13}C_\alpha) > 2.5$ ppm as well as Glu43 showing $\Delta(^1H_N) > 0.2$ ppm and $\Delta(^{15}N) > 1.0$ ppm are due to the mutation of Pro42. In the flexible ω-loop

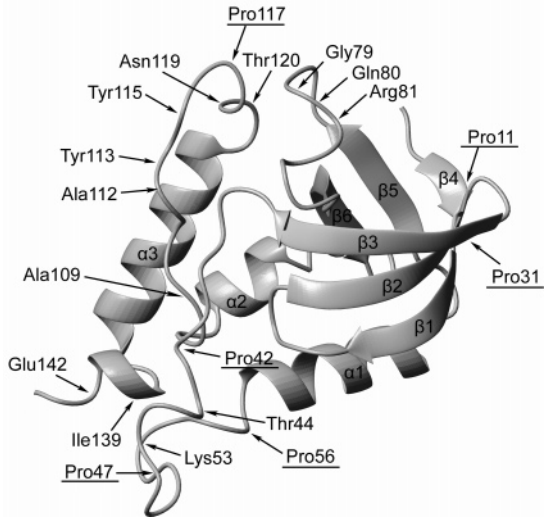

FIGURE 3: Ribbon representation of the SNase structure. Arrows indicate the sites of proline residues and residues showing large chemical shift differences between [Pro$^-$]SNase and SNase.

(Pro42−Pro56), substitution at Pro47 largely influences the chemical shifts of the nearby residues His46 showing $\Delta(^{15}N) > 1.0$ ppm and $\Delta(^{13}C_\alpha) > 1.5$ ppm and Lys48 showing $\Delta(^{15}N) > 1.0$ ppm.

However, substitution at Pro117 caused changes in the chemical shifts not only for nearby residues but also for the residues in distant segments. In the loop of residues Ala112−His121 linking the β-strand (Ala109−Val111) and helix α3 (Glu122−Lys136), the observed chemical shift changes are as follows: $\Delta(^1H_N) > 0.2$ ppm and $\Delta(^1H_\alpha) > 0.2$ ppm for Ala112, $\Delta(^{13}C_\alpha) > 1.5$ ppm for Tyr113, $\Delta(^1H_N) > 0.2$ ppm, $\Delta(^{15}N) > 1.0$ ppm, and $\Delta(^{13}C_\alpha) > 1.5$ ppm for Lys116, $\Delta(^1H_N) > 0.6$ ppm and $\Delta(^{15}N) > 6.0$ ppm for Asn118, $\Delta(^1H_N) > 0.4$ ppm and $\Delta(^{15}N) > 1.0$ ppm for Asn119, and $\Delta(^1H_\alpha) > 0.9$ ppm and $\Delta(^{13}C_\alpha) > 2.0$ ppm for Thr120. Thus, as a consequence of the substitution at Pro117, the great majority of residues in this loop provided large chemical shift changes. Especially, the effect of mutation of Pro117 extended further to residues Ala109 in the short β-strand and Glu124 in helix α3, which provide $\Delta(^{15}N) > 2.0$ ppm and $\Delta(^1H_N) > 0.2$ ppm, respectively. This implies that mutation of Pro117 may induce a conformational change of the Ala112−His121 loop. Particularly, the mutation of Pro117 caused large chemical shift changes for residues in the p-loop[1] (Asp77−Leu89) and the C-terminal loop (Leu137−Glu142) of helix α3 of SNase. Residues Gly79, Gln80, and Arg81 in the p-loop showed large chemical shift changes, which are $\Delta(^1H_N) > 0.4$ ppm for G79, $\Delta(^1H_N) > 0.2$ ppm and $\Delta(^{15}N) > 2.0$ ppm for Gln80, and $\Delta(^{15}N) > 1.0$ ppm and $\Delta(^1H_\alpha) > 0.4$ ppm for Arg81. In the tertiary structure of SNase (*4*), cross-segment hydrogen bonds were identified among residues Glu75, Asp77, Gly79, and Gln80 in the p-loop and Asn118, Asn119, Thr120, and His121 in the loop of residues Ala112−His121. Therefore, the replacement of proline by glycine at position 117 changed not only the backbone conformation of the Ala112−His121 loop but probably the backbone conformation of the p-loop through the hydrogen bond networks between them. The ^1H_N and

[1] Abbreviations: pdTp, thymidine 3′,5′-bisphosphate; p-loop, pdTp-binding loop (Asp77−Leu89).

Table 1: Experimental Constraints and Structural Statistics for the Family of 20 Structures of [Pro$^-$]SNase

parameter	value
constraints used for structure calculation[a]	
intraresidue NOEs ($n = 0$)	799
sequential-range NOEs ($n = 1$)	617
medium-range NOEs ($n = 2-4$)	374
long-range NOEs ($n > 4$)	665
dihedral angle constraints	142
hydrogen bonds	98
total no. of constraints	2695
RMSD from experimental restraints[b]	
distance restraints (Å)	0.0038 ± 0.0005
dihedral angle restraints (deg)	0.1170 ± 0.0193
RMSD from idealized covalent geometry	
bonds (Å)	0.0009 ± 0.00003
angles (deg)	0.2932 ± 0.0024
impropers	0.1257 ± 0.0051
energies (kJ mol^{-1})	
E_{total}	86.92 ± 2.44
E_{VDW}	22.13 ± 1.52
E_{NOE}	2.84 ± 0.80
E_{Cdih}	0.12 ± 0.04
E_{bond}	2.15 ± 0.16
E_{angle}	56.79 ± 0.93
$E_{improper}$	2.89 ± 0.24
Ramachandran analysis[c] (%)	
most favorable region	66.5
additionally allowed	27.8
generously allowed	4.7
disallowed	1.0
average RMSD from the mean NMR structure[d]	
backbone, second structures	0.442
heavy atoms, second structures	1.082
backbone, all residues	2.022
heavy atoms, all residues	2.333

[a] Experimental constraints were imposed on residues His^8−Asp^{143}. [b] RMSD = root-mean-square deviation. No distance restraint was violated by more than 0.5 Å in any of the final structures, and no dihedral angle restraint was violated by more than 5°. [c] Structure quality checks were performed using the program PROCHECK. [d] Backbone atoms include backbone N, C_α, and CO. Heavy atoms include both backbone and side chain non-hydrogen heavy atoms. The term "second structures" means only residues in the secondary structural elements were used. The term "all residues" means all residues in the protein were used.

$^{13}C_\alpha$ resonances of residues Ser141 and Glu142 in the loop of residues Leu137−Glu142 shifted explicitly; $\Delta(^1H_N) > 0.15$ ppm is obtained for both Ser141 and Glu142, and $\Delta(^{13}C_\alpha) > 3.0$ ppm is obtained for Glu142. This means the conformation of the Leu137−Glu142 loop is coupled to the conformation of the Ala112−His121 loop. This is consistent with an early assumption that the long-range structural changes near the C-terminal of SNase are coupled to the configurational state of Lys116−Pro117 (*4*). Therefore, the identified chemical shift differences clearly elucidated the conformational state of [Pro$^-$]SNase.

3D Solution Structure. An ensemble of 20 structures of [Pro$^-$]SNase was converged with a relatively low backbone RMSD and a low target function energy compared to those of the rest of the 180 calculated structures. The number of experimental constraints and structural statistics for [Pro$^-$]SNase are given in Table 1. The distribution of experimental constraints in the primary sequence is shown in Figure 1 of the Supporting Information. The stereochemical quality of the backbone coordinates of the 20 [Pro$^-$]SNase structures was analyzed using the program PROCHECK_NMR (*32*). The results of the Ramanchandran map analysis are given in Table 1. Best-fit superpositions of the backbone heavy atom coordinates of the 20 [Pro$^-$]SNase structures by MOLMOL (*33*) are shown in Figure 4A.

Figure 4B shows superposition of the 3D structures of [Pro$^-$]SNase and SNase. The overall 3D structure of [Pro$^-$]SNase is similar to the solution structure of SNase (PDB code 1J00) (*4*). However, differences in conformation can be observed between [Pro$^-$]SNase and SNase. Explicit local conformational rearrangements were observed for the Ala112−His121 loop and C-terminal α-helical loop of residues Leu137−Glu142 as well as the p-loop of [Pro$^-$]SNase. As compared to the structure of SNase, the Ala112−His121 loop and the p-loop in the tertiary structure of [Pro$^-$]SNas are located closer to each other. The C-terminal Leu137−Glu142 loop of [Pro$^-$]SNase is located closer to the segment of residues Gln106−Leu108, which is a linker between helix α2 and the β-strand of residues Ala109−Val111. The conformational differences of these loops between [Pro$^-$]SNase and SNase are associated with substitution at Pro117 as indicated by the above-described chemical shift changes. It can be seen in Figure 4B that the conformations of the β-strand of residues His8−Ala12, β-turn τ2 (Tyr27−Gln30), helix α1 (Glu57−Ala69), and the short β-strand (Val39−Thr41) showed almost no changes in the structure of [Pro$^-$]SNase compared to the structure of SNase. Therefore, substitutions at residues Pro11, Pro31, Pro56, and Pro42 do not seem to alter the local conformations. Due to the flexibility of the ω-loop in both [Pro$^-$]SNase and SNase, the conformational differences cannot be interpreted for the segment containing mutation site 47.

Backbone Dynamics. The experimental relaxation parameters R_1 and R_2 and $^1H-^{15}N$ NOEs for [Pro$^-$]SNase and SNase are plotted against the residue number in Figure 5. Sequence variations of these relaxation data can be observed for the ω-loop and for the N- and C-terminal regions of residues preceding residue Glu10 and following residue Trp140, respectively. Both the N- and C-terminal regions of the proteins are highly flexible with $^1H-^{15}N$ NOE values <0.6. The approximately similar $^1H-^{15}N$ NOE values in the range 0.43−0.73 but different R_1 and R_2 values are obtained for a number of residues in the ω-loop (Pro42−Pro56) of the proteins. R_1 and R_2 values for residues in the ω-loop of [Pro$^-$]SNase and SNase, respectively, are larger than those for residues in other structural regions, whose R_2 and R_1 values are spread in the approximately same range of numerical values.

The general order parameter, S^2, effective correlation time, τ_e, and R_{ex} term describing the backbone internal motions on fast (nanosecond to picosecond) and slow (millisecond to microsecond) time scales were obtained for [Pro$^-$]SNase and SNase (Figure 5). In the backbone dynamic study, S^2, reflecting fast internal motions, is related to the degree of internal mobility. An S^2 of 0.7 is typically the lower limit for residues in an ordered structural region having restricted internal mobility. Residues with S^2 values well below 0.7 indicate higher internal mobility and flexibility of the corresponding structural region. The N- and C-terminal regions of two proteins are highly flexible, having S^2 values well below 0.7and τ_e times exceeding 500 ps. The S^2 values

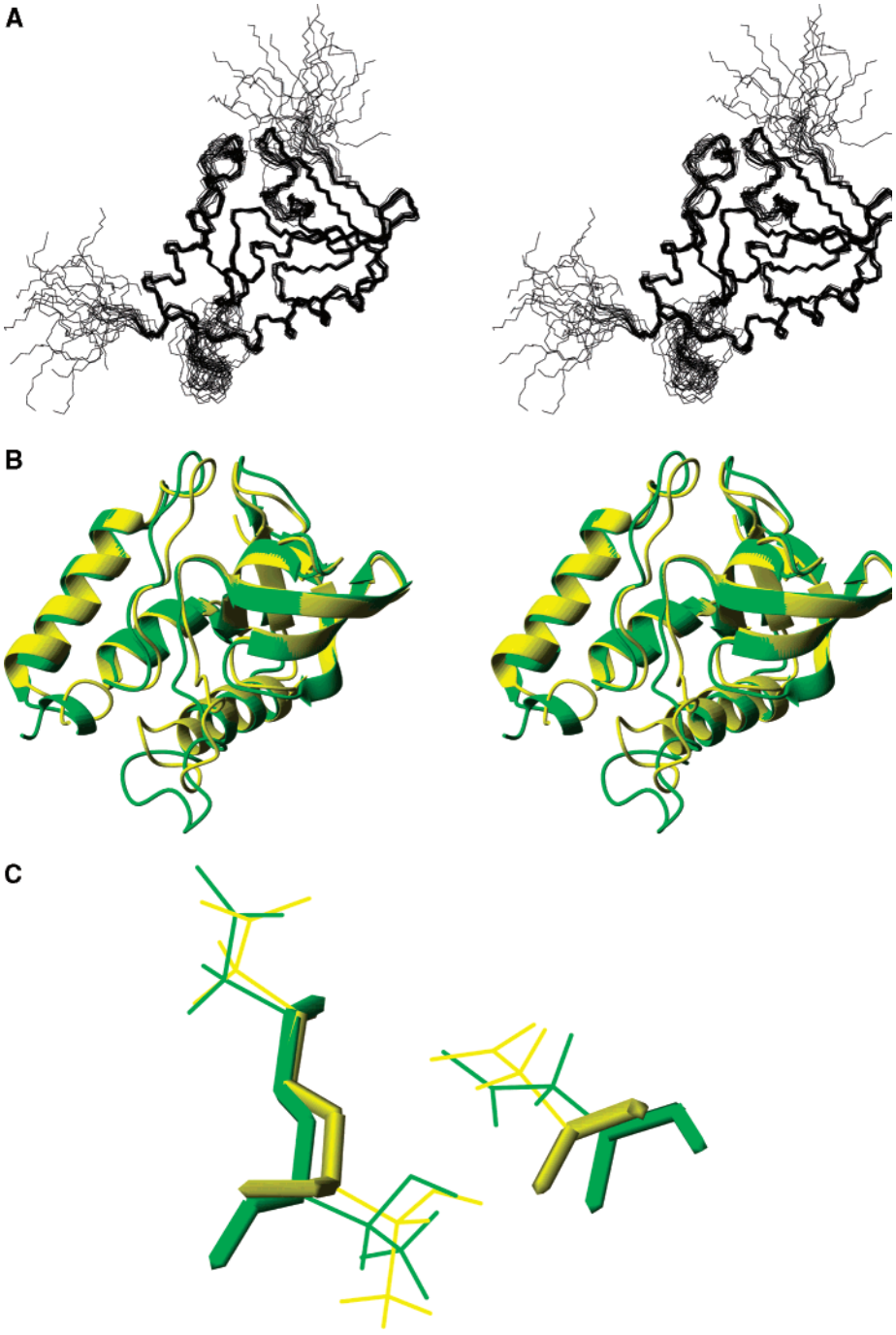

FIGURE 4: NMR-derived structure of [Pro$^-$]Snase: (A) superposition of the 20 structures of [Pro$^-$]Snase; (B) ribbon representation of the superposition of the [Pro$^-$]SNase structure (yellow) on the NMR-derived structure of SNase (green); (C) ribbon representation of the superposition of the Ca^{2+} association site in the [Pro$^-$]SNase structure (yellow) on that in SNase (green). The N-terminal seven residues and the sequence region D143−Q149 of the proteins are not shown.

for the vast majority residues of secondary structural elements including the p-loop and loop of residues Ala112−His121 of [Pro$^-$]SNase and SNase are larger than 0.7 with average values of 0.92 ± 0.07 and 0.91 ± 0.08, respectively. This means the backbone of secondary structural elements including the p-loop and Ala112−His121 loop of [Pro$^-$]SNase and SNase exhibit similar high motional restrictions with a very low degree of internal mobility. The ω-loop of SNase has S^2 values >0.7 but lower than the average value of 0.91 ± 0.08. However, the ω-loop of [Pro$^-$]SNase has S^2 values <0.7 as seen in Figure 5. Thus, the ω-loop in [Pro$^-$]SNase exhibits relatively fast internal motions on the nanosecond to picosecond time scale compared to the motions of the ω-loop in SNase. The different R_{ex} values were obtained for [Pro$^-$]SNase and SNase. R_{ex} is related to slow motions from the interchange between different molecular conformations on the millisecond to microsecond time scale and therefore is correlated to the equilibrium populations of different conformational states. Residues at positions 23, 43, 44, 46, 48, 49, 51, 52, 55, 113, 114, and 120 of SNase and 37, 54, 62, 118, 119, and 120 of [Pro$^-$]SNase showed significant R_{ex} contributions (>3.0 Hz) (Figure 5). It can be seen that the ω-loop of residues Pro42−Pro56 of SNase features a number of contiguous residues having substantial R_{ex} values lying largely between 3.04 and 22.2 Hz. For [Pro$^-$]SNase, among the residues having R_{ex} values >3.0 Hz, only residue

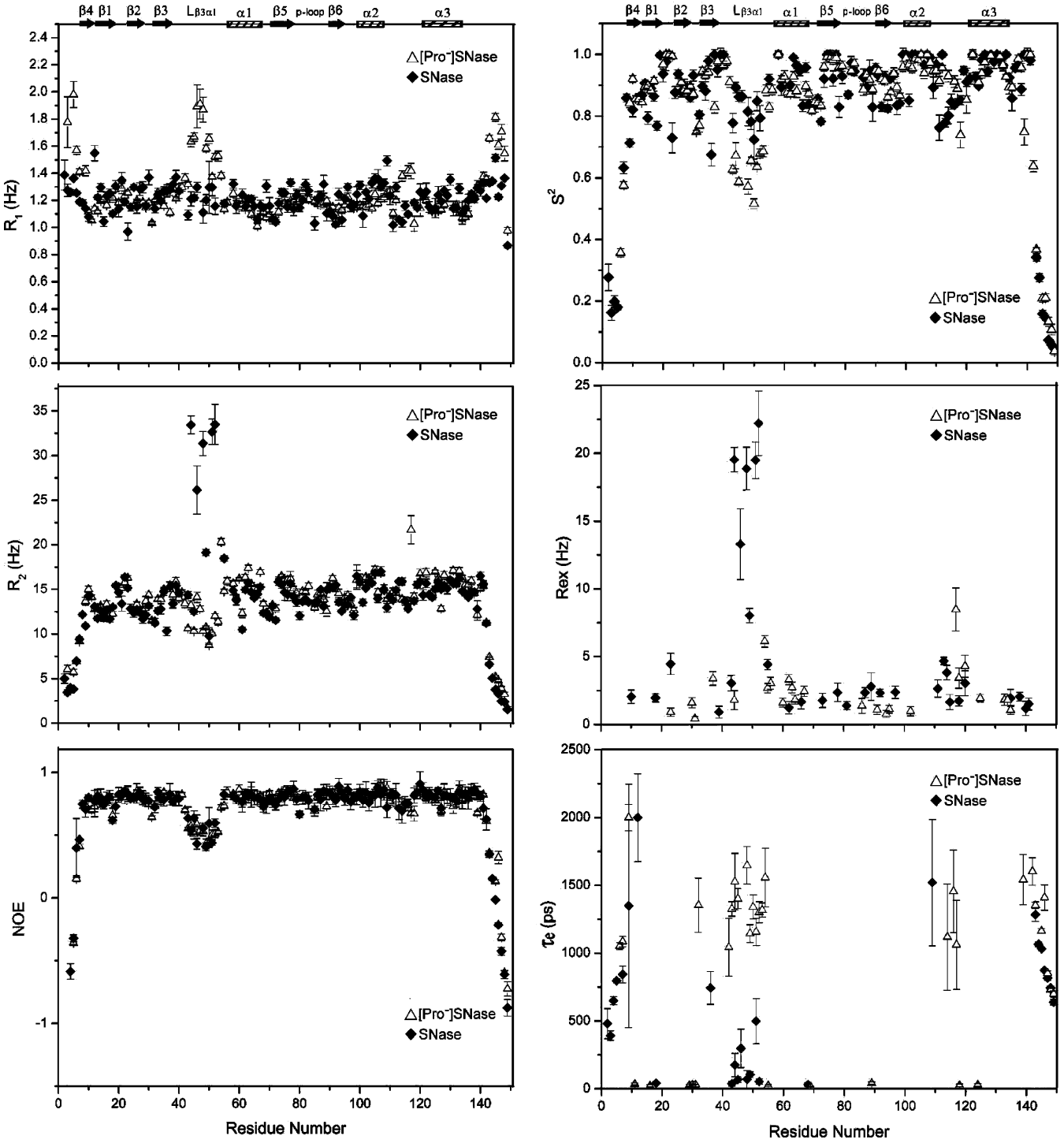

FIGURE 5: Sequence variation of ^{15}N relaxation parameters, R_1 and R_2 rates and ^{15}N NOEs, and model-free parameters, general order parameter, S^2, effective correlation time, τ_e, and exchange rate, R_{ex}, for [Pro$^-$]SNase and SNase at 300 K. The positions of the secondary structures are marked at the top of the figure.

Tyr54 is in the ω-loop. However, many contiguous residues in the ω-loop of [Pro$^-$]SNase have τ_e times in the range 1000−1750 ps (Figure 5). This means the ω-loop in SNase is likely to undergo a higher degree of slow conformational exchange motions on the millisecond to microsecond time scale. In contrast, [Pro$^-$]SNase has a highly flexible ω-loop with very low motional restriction. For the turn region around the residue at position 117 of the Ala112−His121 loop in [Pro$^-$]SNase, R_{ex} contributions in the range 3.0−7.0 Hz were observed for residues at positions 118, 119, and 120, and τ_e times of the residues at positions 115, 117, and 118 were in the range 1000−1500 ps. In SNase, residues at positions 113, 114, and 120 showed R_{ex} values in the range 3.0−5.0 Hz. This indicated that substitution at Pro117 changed the dynamic properties of the peptide bond around position 117. Residues around position 117 in [Pro$^-$]SNase have less restricted internal motions than those in SNase. Therefore, the backbone mobility of the ω-loop and residues around position 117 for [Pro$^-$]SNase is less restricted than that for SNase. However, the p-loop and integrate loop of residues Ala112−His121 exhibit restricted backbone mobility with low flexibility in both [Pro$^-$]SNase and SNase.

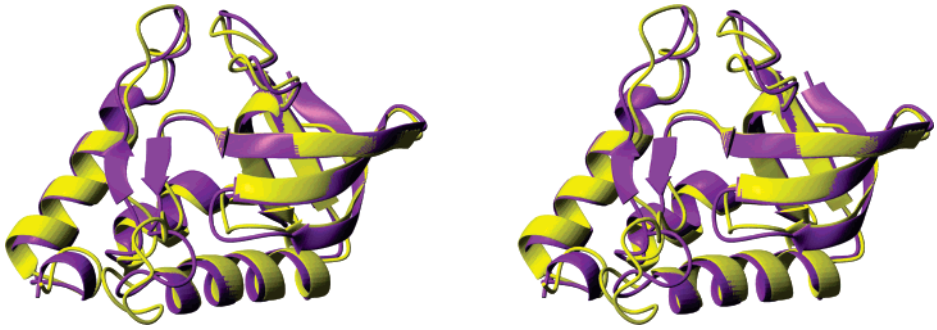

FIGURE 6: Superposition of the [Pro⁻]SNase structure (yellow) on the X-ray structure of P117G-mutant SNase (purple).

DISCUSSION

It was reported that the individual P47G and P117G mutations caused a 7-fold decrease of nuclease activity and increased the protein stability by 0.9 and 1.5 kcal/mol, respectively, whereas the P47G/P117G-doubly-mutant SNase has 1.9% of the activity of the SNase WT (*7*). Thus, the P47G and P117G mutations each cause a small decrease in nuclease activity and have almost the same effect on enzyme activity. Only the P47G/P117G double mutation can cause a significant decrease (about 53-fold) in nuclease activity. [Pro⁻]SNase has approximately the same nuclease activity as the P47G/P117G-doubly-mutant SNase. This suggests that the dramatically decreasing nuclease activity of proline-free mutant SNase is caused mainly by substitutions at residues Pro47 and Pro117 and very little by the other four proline residues. The possible role of Pro11, Pro31, Pro42, and Pro56 in the nuclease activity and molecular stability of SNase seems unimportant. This means the peptidyl−proline bonds of His46−Pro47 and Lys116−Pro117 play an important role in the physiologic function of SNase. Presumably, the cooperative effect of *cis*−*trans* isomerizations of the His46−Pro47 and Lys116−Pro117 peptide bonds on enzyme activity correlates with the backbone conformational and dynamic states of the corresponding segments in SNase.

The Conformational State of the Ala112−His121 Loop Influences the Protein To Exert Function. As was reported, the X-ray structures of P117G-mutant and P47G/P117G-doubly-mutant SNase have very similar tertiary structures. Addition of the P47G mutation appears not to cause any additional structural changes (*7*). Superposition of the NMR-derived structure of [Pro⁻]SNase with the X-ray structure of P117G-mutant SNase (PDB code 1SNP) shows essentially the same backbone orientation except the p-loop and loop of residues Ala112−His121 (Figure 6). However, it is reasonable to observe different loop conformations in solution and in a crystal. Here, the point is that the p-loop and Ala112−His121 loop in both P117G-mutant SNase and [Pro⁻]SNase are located closer to each other compared to those in the crystal structure (*7*) and solution structure (*4*) of native SNase, respectively. This evidenced again that the observed conformational rearrangements in [Pro⁻]SNase are the consequences of substitution at residue 117.

In the tertiary structure of SNase, the cleft formed by the Ala112−His121 loop and p-loop is a putative DNA binding pocket (*4*). The tertiary structure of SNase favors the strained backbone conformation of segment Ala112−Pro117 having a *cis* Lys116−Pro117 peptide with an occupancy of 90% (*9*), which is a favorable conformation for SNase to exert physiological function. Thus, the backbone arrangements of the Ala112−His121 loop and p-loop in the structure of SNase may be most suitable for DNA binding. The rearranged loop conformations as a result of the *trans* Lys116−Gly117 peptide bond in [Pro⁻]SNase must be unfavorable for DNA binding. In SNase, the C-terminal portion constructed by residues Val111−Asp143 (named the α-subdomain) is coupled with the N-terminal main body constructed by residues His8−Val111 (named the *β*-subdomain) through long-range tertiary interactions between them. The hydrogen bond networks are not only formed between the p-loop and Ala112−His121 loop as mentioned above, but also formed by Ile139 N−Gly107 O and Asn138 ND2−Gln106 O between the α-subdomain and *β*-subdomain of the protein (*4*, *34*). The pyrrole ring of Trp140 is surrounded by hydrophobic residues Gly107, Leu108, Ala109, and Ile139 and an amphiphilic residue, Lys133, which form a small hydrophobic core. The hydrogen bond networks and hydrophobic interactions between the α- and *β*-subdomains help to tack the α-subdomain onto the *β*-subdomain of the protein. Many works have contributed to a better understanding of the importance of residue Trp140 for the structure and function of SNase. Mutation of tryptophan at position 140 to amino acids other than histidine dramatically changed the nuclease activity and largely disrupted the structure of SNase (*35*, *36*). This can be attributed to possible changes in the backbone conformation of the Leu137−Glu142 loop as a result of disruption of the long-range tertiary interactions in this area. This means changes in the backbone conformation of the Ala112−His121 loop can transfer to the Leu137−Glu142 loop through helix α3 of residues Glu122−Lys136 and vice versa. Thus, the coupling between α- and *β*-subdomains which is necessary for SNase to exert its function is held by the *cis* Lys116−Pro117 peptide bond. The *trans* Lys116−Pro117 peptide bond, causing conformational rearrangement of the α-subdomain in [Pro⁻]SNase, disrupted this coupling. As a consequence, changes in the coupling between two subdomains either in the DNA binding pocket or in the local structural region of Trp140, resulting from conformational rearrangements, can weaken the binding capability of SNase with DNA, reducing the enzyme activity.

The conformational equilibrium raised by the *cis*−*trans* isomerization of Lys116−Pro117 is reported by residue His121 (*6*, *11*), implying conformational transitions of the Ala112−His121 loop. The dominant conformational state of the Ala112−His121 loop containing the *cis* Lys116−Pro117 peptide bond has a strained backbone conformation in SNase. In [Pro⁻]SNase, the Ala112−His121 loop has a conformation with a *trans* Lys116−Gly117 peptide bond, having no conformational restrictions. At the same time, the backbone

of the segment Tyr115−Asn118 of [Pro$^-$]SNase is more flexible than that of SNase (Figure 5). Such a conformational flexibility of the Ala112−His121 loop facilitates conformational rearrangement of the corresponding segments in the α-subdomain of [Pro$^-$]SNase, influencing coupling with the β-subdomain and reducing the DNA binding capability.

Backbone Dynamic Properties of the ω-Loop Are Important for Enzyme Activity. SNase is a Ca^{2+}-activated extracellular phosphodiesterase, requiring Ca^{2+} ion for degrading both DNA and RNA to 3′-nucleotides. Ca^{2+} ion is coordinated by residues Asp21, Asp40, and Thr41, which are located in β-turn τ1 (Ile18−Asp21) and β-strand Val39−Thr41. The carboxylates of Asp21, Asp40, and Thr41, forming a coordination sphere with a water molecule, are direct ligands of the Ca^{2+} ion (*34*, *37*). The Ca^{2+} coordination site in [Pro$^-$]SNase is very similar to that in SNase (Figure 4C). Thus, substitution at residue Pro42 generates only little influence on the coordination sphere for Ca^{2+} ion in [Pro$^-$]SNase. On the other hand, only mutations of Pro47 and Pro117 but not Pro42 and three other proline residues can give rise to a large effect on nuclease activity. Therefore, decreasing nuclease activity as a result of removing 20% of the *cis*-isomer of the peptidyl−proline bond of Pro47 by substitution at residue 47 may correlate to changes in the backbone dynamic features of the ω-loop.

Analysis of the ^{15}N relaxation data reveals that the ω-loop of SNase undergoes slow conformational exchange motions on the millisecond to microsecond time scale (Figure 5). This means the ω-loop is not completely random in SNase but is in exchange between different molecular conformations. Early dynamic studies on SNase have also reported that Glu52, Lys53, and Tyr54 in the ω-loop have ^{15}N or ^1H_N line widths larger than the average line width obtained from the remainder of the residues, and this is most likely the result of local conformational averaging at a rate comparable to the chemical shift differences of the various conformational forms (*38*). On the other hand, a dual spin system for His46 was observed in the NMR spectrum of SNase, which demonstrated a conformational equilibrium between two substates of the ω-loop due to the *cis*−*trans* isomerization of His46−Pro47 (*5*). Thus, the internal motions of the ω-loop in SNase are hierarchically composed of slow conformational exchange motions on the millisecond to microsecond time scale and conformational transitions raised by the *cis*−*trans* isomerization of His46−Pro47 on the millisecond to second time scale. This suggests that some restrictions are imposed on the backbone of the flexible ω-loop, which shows a restricted motional flexibility in SNase. However, mutation of residue Pro47 to Thr47 removed not only *cis*−*trans* isomerization of His46−Pro47 but also the slow conformational exchange motions on the millisecond to microsecond time scale from internal motions of the ω-loop. The ω-loop in [Pro$^-$]SNase exhibits lower motional restrictions on the nanosecond to picosecond time scale, suggesting that the ω-loop with a *trans* His46−Thr47 peptide bond has a high degree of flexibility (Figure 5). This indicates that the slow conformational exchange motions of the ω-loop are correlated to the X−Pro peptide bond of His46−Pro47. In another words, we can attribute the flexibility restrictions on the ω-loop in SNase to the *cis*−*trans* isomerization of the His46−Pro47 peptide bond.

In the structure of SNase, the ω-loop is not directly involved in the putative DNA binding pocket. However, DNA binding and degradation of SNase must intimately correlate with the ω-loop, since the *cis*- and *trans*-isomers of the His46−Pro47 peptide bond of the ω-loop largely influence the nuclease activity. As is well-known, many enzymatic reactions occur on the millisecond to microsecond time scale. Millisecond to microsecond time scale backbone motions have been observed in binding surfaces for several proteins, suggesting an important role for such motions in molecular recognition. The enzyme cyclophilin A (CypA) catalyzes the *cis*−*trans* isomerization of the Phe−Pro peptide bond of the substrate. Slow conformational exchange motions on the millisecond to microsecond time scale were detected for the active site of the enzyme. The backbone amide nitrogen of Arg55 clearly experiences conformational exchange motions associated with the isomerization and binding process (*39*). The three different complexes of *Escherichia coli* dihydrofolate reductase, E:folate:$NADP^+$, E:folate, and E:folate:DHNADPH, represent different stages in the catalytic cycle of the enzyme. Differences in the millisecond to microsecond time scale motions are evident from significant changes in the R_{ex} terms among the three complexes. Millisecond to microsecond time scale slow conformational exchange motions occur within the adenosine binding pocket or even in transient dissociation of the adenosine moiety itself (*40*). Apparently, internal protein dynamics are intimately connected to enzymatic catalysis. Thus, the flexibility restrictions of the ω-loop may be important for SNase to bind with DNA. In contrast, a highly flexible ω-loop in [Pro$^-$]SNase may be unfavorable for DNA binding.

Interestingly, the flexibility of loops forming the binding pocket is necessary in vivo to make the binding site accessible to a ligand. Such loops may be mobile on the fast nanosecond time scale for lack of structure information and may order upon binding of ligand molecules. However, the loops forming the DNA binding pocket or involved in the binding of DNA have no sufficient flexibility in SNase. The backbone of the p-loop exhibits restricted mobility, and the integrated Ala112−His121 loop has restricted conformational flexibility, whereas the ω-loop undergoes slow conformational exchange motions on the millisecond to microsecond time scale, showing restricted backbone flexibility in SNase. Probably, loops in the DNA binding surface with certain degrees of restriction on motional flexibility and conformational flexibility are the inherent features for SNase to exert enzyme function.

ACKNOWLEDGMENT

We thank Professor K. Kuwajima (University of Tokyo) for kindly providing the plasmid of wild-type proline-free staphylococcal nuclease.

SUPPORTING INFORMATION AVAILABLE

One figure showing the distribution of experimental constraints in the primary sequence. This material is available free of charge via the Internet at http://pubs.acs.org.

REFERENCES

1. Nall, B. T. (1994) in *Mechanisms of Protein Folding: Frontiers in Molecular Biology* (Pain, R. H., Ed.) pp 80−103, Oxford University Press, New York.

2. Brandl, C. J., and Deber, C. M. (1986) Hypothesis about the function of membrane-buried proline residues in transport proteins, *Proc. Natl. Acad. Sci. U.S.A. 83*, 917−921.
3. Hynes, T. R., and Fox, R. O. (1991) The crystal structure of staphylococcal nuclease refined at 1.7 A resolution, *Proteins 10*, 92−105.
4. Wang, J., Truckses, D. M., Abildgaard, F., Dzakula, Z., Zolnai, Z., and Markley, J. L. (1997) Solution structures of staphylococcal nuclease from multidimensional, multinuclear NMR: nuclease-H124L and its ternary complex with Ca^{2+} and thymidine-3′,5′-bisphosphate, *J. Biomol. NMR 10*, 143−164.
5. Loh, S. N., McNemar, C. W., and Markley, J. L. (1991) Detection and kinetic characterization of a novel proline isomerism in staphylococcal nuclease by NMR spectroscopy, *Techniques in Protein Chemistry*, Vol. 11, pp 275−282, Academic Press, Inc., New York.
6. Evans, P. A., Dobson, C. M., Kautz, R. A., Hatfull, G., and Fox, R. O. (1987) Proline isomerism in staphylococcal nuclease characterized by NMR and site-directed mutagenesis, *Nature 329*, 266−268.
7. Truckses, D. M., Somoza, J. R., Prehoda, K. E., Miller, S. C., and Markley, J. L. (1996) Coupling between trans/cis proline isomerization and protein stability in staphylococcal nuclease, *Protein Sci. 5*, 1907−1916.
8. Hodel, A., Kautz, R. A., Jacobs, M. D., and Fox, R. O. (1993) Stress and strain in staphylococcal nuclease, *Protein Sci. 2*, 838−850.
9. Hodel, A., Kautz, R. A., Adelman, D. M., and Fox, R. O. (1994) The importance of anchorage in determining a strained protein loop conformation, *Protein Sci. 3*, 549−556.
10. Alexandrescu, A. T., Mills, D. A., Ulrich, E. L., Chinami, M., and Markley, J. L. (1988) NMR assignments of the four histidines of staphylococcal nuclease in native and denatured states, *Biochemistry 27*, 2158−2165.
11. Alexandrescu, A. T., Ulrich, E. L., and Markley, J. L. (1989) Hydrogen-1 NMR evidence for three interconverting forms of staphylococcal nuclease: effects of mutations and solution conditions on their distribution, *Biochemistry 28*, 204−211.
12. Alexandrescu, A. T., Hinck, A. P., and Markley, J. L. (1990) Coupling between local structure and global stability of a protein: mutants of staphylococcal nuclease, *Biochemistry 29*, 4516−4525.
13. Feng, Y., Liu, D., and Wang, J. (2003) Native-like partially folded conformations and folding process revealed in the N-terminal large fragments of staphylococcal nuclease: a study by NMR spectroscopy, *J. Mol. Biol. 330*, 821−837.
14. Wang, X., Tong, Y., and Wang, J. (2005) Cis/trans heterogeneity of Gln30-Pro31 peptide bond determines whether a 79-residue fragment of staphylococcal nuclease self-associates, *Biochem. Biophys. Res. Commun. 329*, 495−501.
15. Walkenhorst, W. F., Green, S. M., and Roder, H. (1997) Kinetic evidence for folding and unfolding intermediates in staphylococcal nuclease, *Biochemistry 36*, 5795−5805.
16. Maki, K., Ikura, T., Hayano, T., Takahashi, N., and Kuwajima, K. (1999) Effects of proline mutations on the folding of staphylococcal nuclease, *Biochemistry 38*, 2213−2223.
17. Kamagata, K., Sawano, Y., Tanokura, M., and Kuwajima, K. (2003) Multiple parallel-pathway folding of proline-free Staphylococcal nuclease, *J. Mol. Biol. 332*, 1143−1153.
18. Sarkar, G., and Sommer, S. S. (1990) The "megaprimer" method of site-directed mutagenesis, *Biotechniques 8*, 404−407.
19. Ye, K., Jing, G., and Wang, J. (2000) Interactions between subdomains in the partially folded state of staphylococcal nuclease, *Biochim. Biophys. Acta 1479*, 123−134.
20. Cuatrecasas, P., Fuchs, S., and Anfinsen, C. B. (1967) Catalytic properties and specificity of the extracellular nuclease of Staphylococcus aureus, *J. Biol. Chem. 242*, 1541−1547.
21. Wang, J. F., Mooberry, E. S., Walkenhorst, W. F., and Markley, J. L. (1992) Solution studies of staphylococcal nuclease H124L. 1. Backbone 1H and 15N resonances and secondary structure of the unligated enzyme as identified by three-dimensional NMR spectroscopy, *Biochemistry 31*, 911−920.
22. Wang, J. F., Hinck, A. P., Loh, S. N., LeMaster, D. M., and Markley, J. L. (1992) Solution studies of staphylococcal nuclease H124L. 2. 1H, 13C, and 15N chemical shift assignments for the unligated enzyme and analysis of chemical shift changes that accompany formation of the nuclease-thymidine 3′,5′-bisphosphate-calcium ternary complex, *Biochemistry 31*, 921−936.
23. Zhu, G., and Bax, A. (1992) Improved linear prediction of damped NMR signals using modified forward back linear prediction, *J. Magn. Reson. 100*, 202−207.
24. Markley, J. L., Bax, A., Arata, Y., Hilbers, C. W., Kaptein, R., Sykes, B. D., Wright, P. E., and Wuthrich, K. (1998) Recommendations for the presentation of NMR structures of proteins and nucleic acids. IUPAC-IUBMB-IUPAB Inter-Union Task Group on the Standardization of Data Bases of Protein and Nucleic Acid Structures Determined by NMR Spectroscopy, *J. Biomol. NMR 12*, 1−23.
25. Farrow, N. A., Muhandiram, R., Singer, A. U., Pascal, S. M., Kay, C. M., Gish, G., Shoelson, S. E., Pawson, T., Forman-Kay, J. D., and Kay, L. E. (1994) Backbone dynamics of a free and phosphopeptide-complexed Src homology 2 domain studied by 15N NMR relaxation, *Biochemistry 33*, 5984−6003.
26. Cornilescu, G., Delaglio, F., and Bax, A. (1999) Protein backbone angle restraints from searching a database for chemical shift and sequence homology, *J. Biomol. NMR 13*, 289−302.
27. Brunger, A. T., Adams, P. D., Clore, G. M., DeLano, W. L., Gros, P., Grosse-Kunstleve, R. W., Jiang, J. S., Kuszewski, J., Nilges, M., Pannu, N. S., Read, R. J., Rice, L. M., Simonson, T., and Warren, G. L. (1998) Crystallography & NMR system: A new software suite for macromolecular structure determination, *Acta Crystallogr., D: Biol. Crystallogr. 54*, 905−921.
28. Palmer, A. G., Rance, M., and Wright, P. E. (1991) Intramolecular motions of a zinc finger DNA-binding domain from Xfin characterized by proton-detected natural abundance carbon-13 heteronuclear NMR spectroscopy, *J. Am. Chem. Soc. 113*, 4371−4380.
29. Dosset, P., Hus, J. C., Blackledge, M., and Marion, D. (2000) Efficient analysis of macromolecular rotational diffusion from heteronuclear relaxation data, *J. Biomol. NMR 16*, 23−28.
30. Lipari, G., and Szabo, A. (1982) Model-free approach to the interpretation of nuclear magnetic resonance relaxation in macromolecules. 1. Theory and range of validity, *J. Am. Chem. Soc. 104*, 4546−4559.
31. Xie, T., Liu, D., Feng, Y., Shan, L., and Wang, J. (2007) Folding stability and cooperativity of the three forms of 1−110 residues fragment of staphylococcal nuclease, *Biophys. J. 92*, 2090−2107.
32. Laskowski, R. A., Rullmannn, J. A., MacArthur, M. W., Kaptein, R., and Thornton, J. M. (1996) AQUA and PROCHECK-NMR: programs for checking the quality of protein structures solved by NMR, *J. Biomol. NMR 8*, 477−486.
33. Koradi, R., Billeter, M., and Wuthrich, K. (1996) MOLMOL: a program for display and analysis of macromolecular structures, *J. Mol. Graphics 14*, 51−32.
34. Loll, P. J., and Lattman, E. E. (1989) The crystal structure of the ternary complex of staphylococcal nuclease, Ca^{2+}, and the inhibitor pdTp, refined at 1.65 A, *Proteins 5*, 183−201.
35. Hirano, S., Mihara, K., Yamazaki, Y., Kamikubo, H., Imamoto, Y., and Kataoka, M. (2002) Role of C-terminal region of staphylococcal nuclease for foldability, stability, and activity, *Proteins 49*, 255−265.
36. Hirano, S., Kamikubo, H., Yamazaki, Y., and Kataoka, M. (2005) Elucidation of information encoded in tryptophan 140 of staphylococcal nuclease, *Proteins 58*, 271−277.
37. Cotton, F. A., Hazen, E. E., Jr., and Legg, M. J. (1979) Staphylococcal nuclease: proposed mechanism of action based on structure of enzyme-thymidine 3′,5′-bisphosphate-calcium ion complex at 1.5-A resolution, *Proc. Natl. Acad. Sci. U.S.A. 76*, 2551−2555.
38. Kay, L. E., Torchia, D. A., and Bax, A. (1989) Backbone dynamics of proteins as studied by ^{15}N inverse detected heteronuclear NMR spectroscopy: Application to staphylococcal nuclease, *Biochemistry, 28*, 8972−8979.
39. Eisenmesser, E. Z., Bosco, D. A., Akke, M. and Kern, D. (2002) Enzyme dynamics during catalysis, *Science 295*, 1520−1523.
40. Osborne, M. J., Schnell, J., Benkovic, S. J., Dyson, H. J. and Wright, P. E. (2001) Backbone dynamics in dihydrofolate reductase complexes: role of loop flexibility in the catalytic mechanism, *Biochemistry 40*, 9846−9859.

BI7009794